

## DTA STUDY OF THE CHLORINATION OF FLY ASH AND BAUXITE IN THE PRESENCE OF CARBON

TADA0 ISHII, TAKESHI TSUCHIDA, RYUSABURO FURUICHI, HIROSHI HAGA  
and KAZUHIKO KUDO

*Department of Applied Chemistry, Faculty of Engineering, Hokkaido University, Sapporo 060 (Japan)*

(Received 28 July 1981)

### ABSTRACT

The chlorination processes of fly ash and bauxite in the presence of carbon were studied by means of a gas-flow type DTA, X-ray analysis and SEM observation, and the reactivity of Al-compounds as their constituents was compared. In the case of fly ash, the exothermic peak due to the formation of  $\text{AlCl}_3$  (mainly) and  $\text{FeCl}_3$  appeared at about 790–920°C. The reactivity of Al estimated from the DTA peak temperature depended on the particle size, carbon content and preparation temperature of fly ash, and was much lower than that of bauxite. Fractional conversion of Al was about 60–70%, when fly ash (–300 mesh) was heated up to 900°C in  $\text{Cl}_2$  at 5°C  $\text{min}^{-1}$  of heating rate. In the case of bauxite, two exothermic peaks due to the chlorination of Fe and Al appeared at about 270 and 490°C, respectively. The chlorination of Al was completed at 550°C under the above conditions.

### INTRODUCTION

In recent years there has been an increasing number of studies made to use fly ash in a more productive manner. Simons et al. [1] tentatively concluded on the basis of X-ray study of fly ash that there is a positive correlation between pozzolanic activity (reactivity with lime in the presence of water) and glass content. The proportion of glass in nine fly ashes was greater than 50%, and quartz and mullite were the main crystalline constituents. Cavin et al. [2] reported the composition and physical properties as a basis for research on iron and aluminum recovery from the fly ash. X-Ray diffraction patterns revealed the crystalline component of fly ash to be primarily mullite, with the presence of hematite, magnetite, silica and gypsum. Landsberg [3] studied the chlorination of low-grade bauxite and kaolin clay to determine the potential of these materials as sources of aluminum chloride. Gamma alumina, which can be prepared from bauxite or clay, offered the best potential for chlorination. Kaolin was chlorinated in a complex manner at a much slower rate. Murtha et al. [4] concluded that iron and aluminum constituents can be recovered from glassy fly ash by a chlorination process at 700–970°C. The glassy nature of the fly ash makes it less reactive than an ore material, but 56% of the aluminum and 90% of iron were recovered at 970°C of chlorination temperature. Mehrotra et al. [5]

indicated that the chlorination route in the presence of a reducing agent for the metal recovery from coal ash is feasible over a wide temperature range, on the basis of the thermodynamic study of the reaction system for 135 chemical species containing 12 elements. However, these papers shown above suggest, as concluded by Simons et al. [1], that fly ash is such a very complex material, in which the overall chemical composition, amount and composition of glass and the mineral composition of the crystalline fraction vary from particle to particle, and that its characterization in detail for the chlorinating reactivity would be extremely difficult.

In our previous works [6,7], a simple gas-flow DTA apparatus with a flow system, by which  $\text{Cl}_2$ -gas can flow through the reference and the sample powder beds, has been developed and applied to the studies of the chlorination of various Mg-containing ores (olivine, protoenstatite and talc), hydrated aluminas (bayerite, gibbsite, pseudoboehmite and boehmite) and transition aluminas ( $\eta$ -,  $\gamma$ -,  $\delta$ -, and  $\theta$ - $\text{Al}_2\text{O}_3$ ) in the presence of active carbon. Furthermore, this apparatus has also been applied to the study of the chlorination process of bauxite and its constituents such as hydrated alumina, hematite and their mixtures [8]. These results showed that DTA study as a non-isothermal experimental technique is useful to characterize the reactivity of such a complex material over the wide temperature range.

In this paper, the chlorination process of fly ash was studied by means of this gas-flow type DTA, X-ray analysis and electron microscopic observation, and the reactivity of aluminum compounds as its constituents for the chlorination was compared with that of bauxite.

## EXPERIMENTAL

### Materials

Fly ash was obtained from Toyonuma power station, Hokkaido Electric Power Co. Fly ash-EP and fly ash-MC samples are the materials collected from the electrical precipitator and the multiple cyclone separator, respectively. The analysis of  $\text{Al}_2\text{O}_3$ ,  $\text{Fe}_2\text{O}_3$ ,  $\text{TiO}_2$ ,  $\text{CaO}$  and  $\text{MgO}$  was carried out according to JIS [9], that of  $\text{SiO}_2$  and ignition loss (at  $750^\circ\text{C}$  for 1 h) to JIS [10]. The results are shown in Table 1.

TABLE I  
Analysis of fly ash (wt %)

Samples	Mesh	$\text{SiO}_2$	$\text{Al}_2\text{O}_3$	$\text{Fe}_2\text{O}_3$	$\text{TiO}_2$	$\text{CaO}$	$\text{MgO}$	$I_g$ loss	$I_M/I_Q$
EP	-300	56.7	25.9	4.2	1.6	1.5	1.1	0.3	0.56
MC <sub>1</sub>	+100		25.6		0.6		1.5	0.3	0.51
MC <sub>2</sub>	-100 + 200		25.9		0.7		1.5	0.3	0.51
MC <sub>3</sub>	-200 + 300		24.9		0.8		1.8	0.4	0.59
MC <sub>4</sub>	-300		24.7		0.8		2.0	0.5	0.52

No significant difference in the  $\text{Al}_2\text{O}_3$  content of all the samples was noted. Accordingly, the value of 25.9% for  $\text{Al}_2\text{O}_3$  was used as the criterion for estimating the fractional conversion by chlorination of the aluminum. Loss by ignition was small and so the carbon remaining is negligible.  $I_M/I_Q$  estimated from X-ray analysis was used for evaluating the difference in the phase composition of the sample, where  $I_M$  and  $I_Q$  are the X-ray diffraction intensities for mullite ( $2\theta = 26.27^\circ$ ,  $d = 3.390 \text{ \AA}$ ) and quartz ( $2\theta = 26.64^\circ$ ,  $d = 3.343 \text{ \AA}$ ), respectively. No significant difference in X-ray analysis is recognized for any of the samples.

Mullite was prepared by reference to the paper of Ghate et al. [11]. Two mixtures (mixing ratio = 3:2) of activated alumina ( $\gamma\text{-Al}_2\text{O}_3$ , Merck) and amorphous silica (Kanto, GR) were calcined at  $1550^\circ\text{C}$  for 1 h and  $1400^\circ\text{C}$  for 2 h, respectively. The resulting mullites contained a residual  $\alpha\text{-Al}_2\text{O}_3$  phase. The mullitization of the kaolin mineral (Kondo Kogyo) was used to prepare the other mullite. Kaolin calcined at  $1400^\circ\text{C}$  for 2 h contained the cristobalite phase, while that calcined at  $1200^\circ\text{C}$  for 1 h contained quartz and resembled closely the X-ray diffraction pattern of fly ash.

Bauxite was obtained from the Nippon Keikinzoku Co., and ground to pass through a 200 mesh sieve. The analysis (in Table 2) was carried out according to the prescribed method [12]. X-Ray diffraction peaks of gibbsite and hematite were recognized as crystalline hydrated alumina and iron oxide, respectively.

Gibbsite, which is a constituent of bauxite, was prepared from an aqueous solution of sodium aluminate [2].

Hematite was prepared by calcining  $\text{Fe}(\text{OH})_3$  at  $600^\circ\text{C}$  for 3 h in air.

Active carbon (Kanto) was used as a reducing reagent.

### DTA experiments

The gas-flow DTA apparatus used for chlorinating the materials consisted of two quartz tubes (i.d. = 10 mm) placed vertically in a furnace, the one was used as a reference cell and the other as a sample cell.  $\text{Cl}_2$  gas was made to flow through the reference and sample powders during the chlorination experiments. Chromel–alumel thermocouples ( $d = 0.3 \text{ mm}$ ) were protected by a fine quartz tube (o.d. = 4.5 mm) from corrosive atmospheric gas such as  $\text{Cl}_2$  and they were placed at the center of sample and reference beds. Active carbon was thoroughly mixed with the material in a rotating V-type micro mixer (Tsutsui Rikagaku) for 1 h. In the standard DTA experiments, total sample weight (containing carbon) of 500–700 mg, heating rate of  $5^\circ\text{C min}^{-1}$  and  $\text{Cl}_2$  gas flow rate of  $30 \text{ cm}^3 \text{ min}^{-1}$  were employed.

In order to analyse the samples in the course of DTA runs, the samples heated up

TABLE 2

Analysis of bauxite (wt %)

$\text{Al}_2\text{O}_3$	$\text{Fe}_2\text{O}_3$	$\text{SiO}_2$	$\text{TiO}_2$	Ig loss
54.0	8.2	4.5	1.0	30.3

to various temperatures were rapidly quenched to room temperature after the cell was taken out of the furnace. A stream of  $N_2$  gas was passed through the apparatus to stop the reaction and to displace  $Cl_2$  prior to quenching the sample. The chlorides of constituents in the samples were dissolved in water, the  $Al_2O_3$  and  $Fe_2O_3$  in the residues were analysed quantitatively to estimate their fractional conversions and the  $Al^{3+}$  and  $Fe^{3+}$  in the solutions were analysed qualitatively. Chlorination products condensed near the cool end of the sample cell were analysed by the X-ray method.

## RESULTS AND DISCUSSION

### *Chlorination-DTA of fly ash*

Figure 1 shows the DTA curves of fly ash-EP (-300 mesh) with the various carbon contents (C/EP, by weight) in a  $Cl_2$  flow. In the temperature range below  $700^\circ C$  (not shown in the figure), an exothermic peak due to the adsorption of  $Cl_2$  and an endothermic peak due to the dehydration of the sample appeared below  $200^\circ C$ . In the case of a flowing- $N_2$  atmosphere, however, only one large endothermic peak appeared at about  $90^\circ C$ . The amount of fly ash used was 400 mg except for curves (b) and (g) (800 and 740 mg). Curve (a) shows the DTA curve of C/EP = 0 (without carbon). As there is no exothermic peak below  $900^\circ C$  (and fractional

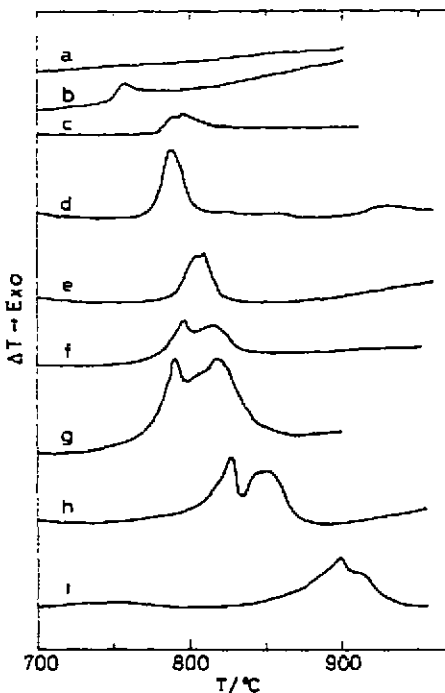


Fig. 1. DTA curves of fly ash-EP (-300 mesh) with carbon (C/EP, by weight) in a  $Cl_2$  flow. C/EP: a, 0; b, 0, c, 0.125, d, 0.25; e, 0.333; f, 0.5; g, 0.5, h, 1.0, i, 2.0. Sample weight: 400 mg except for b (800 mg) and g (740 mg).

conversion, Fig. 4), it is considered that chlorination does not occur without carbon. Curves (c)–(i) show DTA curves of the samples with the various carbon contents. Generally, the exothermic peak from the overlapping of two exothermic peaks appears at about 790–900°C. The lowest peak temperature appears at 790°C in curve (d) ( $C/EP = 0.25$ ) and increasing the  $C/EP$  value tends to shift this peak to a higher temperature. The brown-yellow and yellow condensates are deposited near the cool end of the sample cell, as the exothermic peak begins. A qualitative analysis of the condensates showed the presence of  $Al^{3+}$  and  $Fe^{3+}$ , so that this exothermic peak seems to be due to the formation of  $AlCl_3$  (mainly) and  $FeCl_3$ . The behavior of the exothermic peak in curve (f) corresponds to the result of the conversion–temperature curve shown in Fig. 4. By considering SEM observations of the samples after the chlorination (Fig. 9), it can be estimated that the 1st and 2nd peaks of the exothermic peak probably correspond to the reaction proceeding at the surface and that leading towards bulk product formation, respectively. The reason why this exothermic peak shifts to the higher temperature with increasing carbon content is not understood. However, it is at least not thought that this tendency results from the increasing of the overall sample amount due to adding the carbon, since there is no difference between the peak temperatures of curve (f) (600 mg of sample with carbon) and curve (g) (1110 mg), though the former peak is smaller than the latter.

Curve (b) shows the DTA curve of the sample  $C/EP = 0$ , which used double the weight of EP sample used in curve (a). A small exothermic peak appears at about 750°C, in contrast with curve (a). The qualitative analysis of the condensate formed near the cool end of the sample cell showed the presence of only the  $Fe^{3+}$  ion and no  $Al^{3+}$ . The crystalline iron oxide present in the fly ash was not identified by X-ray analysis (in Fig. 6). However, Simons et al. [1] have reported that iron occurs in fly ash as crystalline components (mainly magnetite and hematite) and as glass. Okahara et al. [13] showed that, by the TG experiments, the chlorination of wustite, magnetite and ferric oxide without a reducing reagent occurs at 270, 300 and 700°C, and these iron oxides are oxidized according to the process,  $FeO \rightarrow Fe_3O_4 \rightarrow Fe_2O_3$ , respectively. On the basis of these results, it is thought that the exothermic peak in curve (b) corresponds to the chlorination of hematite to  $FeCl_3$ . Okahara et al. have also recognized the great promoting effect of carbon in the chlorination of iron oxides. In our works, however, the condensate containing  $Fe^{3+}$  was formed at the initial temperature of the exothermic peak in curves (c)–(i). This suggests that a glassy nature of the fly ash makes it less reactive than a crystalline material.

Figure 2 shows the DTA curves of fly ash-MC (800 mg) with carbon ( $C/MC = 0.25$ ) in a  $Cl_2$  flow. The particle size is altered in the range of +100 to –300 mesh. Compared with the results for fly ash-EP in Fig. 1, the shape of the exothermic peak is analogous but its position shifts to a higher temperature.

Figure 3 (n)–(q) show the DTA curves of fly ash-MC (400 mg) with  $C/MC = 0.5$  instead of  $C/MC = 0.25$  as in Fig. 2. As the particle size becomes smaller, the peak temperature shifts to a somewhat lower temperature and the peak height becomes progressively larger. Compared with the results in Fig. 2, the peak shifts to a higher temperature, due to the increasing carbon content. Figure 3(r) shows the result for

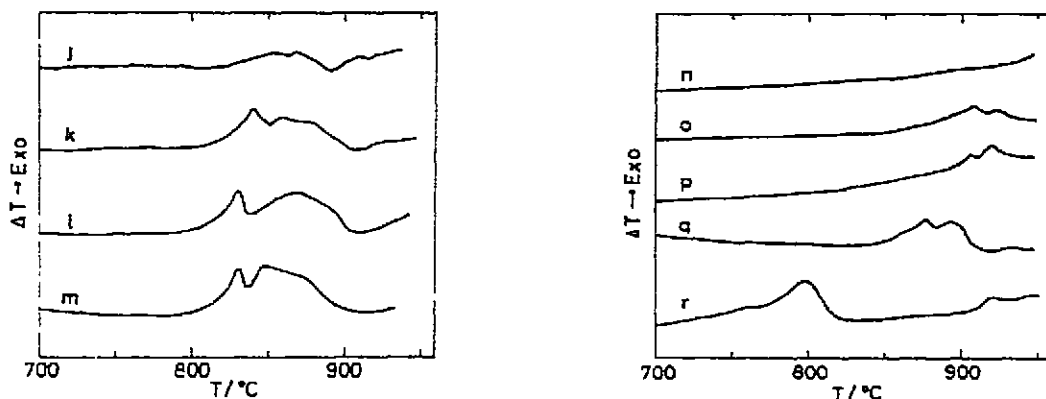


Fig 2 DTA curves of fly ash-MC (800 mg) with carbon ( $C/MC=0.25$ ) in a  $Cl_2$  flow Particle size (mesh) j, +100, k, -100 +200, l, -200 +300, m, -300

Fig 3 DTA curves of fly ash-MC (400 mg) with carbon ( $C/MC=0.5$ ) in a  $Cl_2$  flow Particle size (mesh) n, +100, o, -100 +200, p, -200 +300; q, -300, r, -300 (prepared by grinding fly ash-MC (+100 mesh) to -300 mesh)

the sample prepared by grinding the fly ash-MC (+100 mesh) used in curve (n) to pass through -300 mesh sieve. This curve is analogous to curve (f) for fly ash-EP (-300 mesh) in Fig. 1. On the basis of these results, it is thought that the difference in reactivity between fly ash-EP and -MC is attributable to particle size only. The fractional conversions of aluminum at 950°C after the chlorination-DTA in Fig. 3 were 32.0, 49.4, 47.8, 54.3 and 59.0% for curves (n), (o), (p), (q) and (r), respectively.

Figure 4 shows the fractional conversions for the chlorination of the aluminum in fly ash-EP (-300 mesh) and -MC (-300 mesh) which were taken at the various temperatures of the DTA curves (a), (d) and (f) in Fig. 1 and curve (q) in Fig. 3. Comparing the curve in Fig. 4 with the exothermic peak of curve (f) in Fig. 1, it is estimated that about 25% of aluminum converts at the 1st peak due to the surface reaction accompanying the surface area increase, followed by the conversion up to about 60% at the 2nd peak and then a very slow reaction over the temperature range above the exothermic peak. The fractional conversion of the EP sample (-300 mesh) without carbon ( $C/EP=0$ ) is 6.6% at 900°C, and this is comparable with the value (6.9%) for the same sample with carbon ( $C/EP=0.5$ ) in a flowing  $N_2$  atmosphere. Therefore, it is thought that the value of 6.6% is due to some unknown factor other than the chlorination.

Figure 5 shows the effect of particle size on the fractional conversions for the chlorination of the MC sample with carbon ( $C/MC=0.5$ ) at temperatures of 940–956°C as in the DTA experiments in Fig. 3. The value for the sample (-300 mesh) prepared by grinding MC sample (+100 mesh) is approximately the same as for the EP sample (-300 mesh). This means the reactivity of fly ash depends greatly on the particle size, as considered previously.

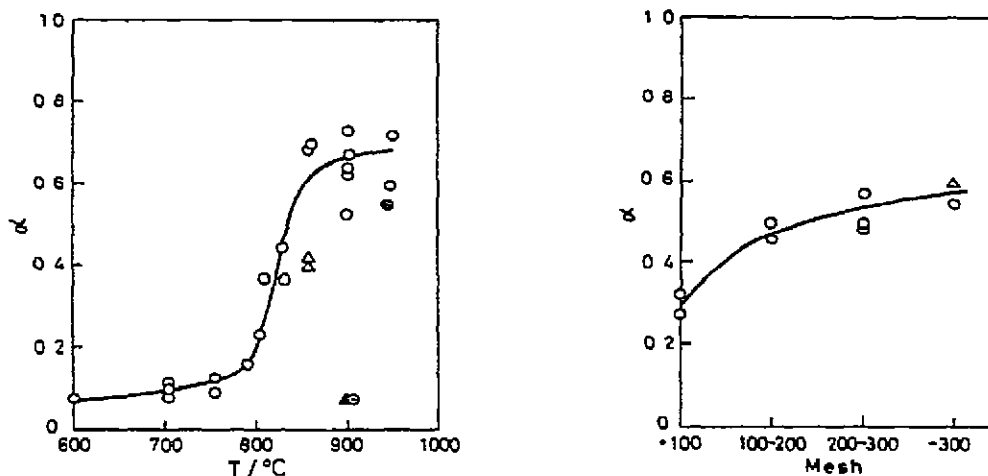


Fig 4 The relationships between fractional conversion and temperature for the chlorination of aluminum in fly ash-EP ( $-300$  mesh) in Fig 1 (a, d and f) and fly ash-MC ( $-300$  mesh) in Fig 3(q) C/EP(MC):  $\circ$ , 0.5,  $\triangle$ , 0.25;  $\bullet$ , 0.5 (MC)  $\blacktriangle$ , 0,  $\circ$ , 0.5 (in a  $N_2$  flow)

Fig 5 The effect of particle size on the fractional conversions for the chlorination of fly ash-MC ( $\circ$ ) with carbon (C/MC=0.5) at temperatures of  $940$ – $956^\circ\text{C}$   $\triangle$ , prepared by grinding MC sample ( $+100$  mesh) to  $-300$  mesh

#### *X-Ray analysis, SEM and EPMA observations of fly ash*

Figure 6 shows the X-ray diffraction patterns of fly ash before and after the chlorination. F-a shows the peaks of quartz and mullite present in the original fly ash-EP ( $-300$  mesh) sample. F-b shows the pattern of fly ash-MC prepared by grinding MC ( $+100$  mesh) to pass through a  $-300$  mesh sieve. This pattern is approximately the same as that of F-a, though the crystallinity of mullite is somewhat low. These results suggest that there are no significant differences between the crystalline structures of EP and MC, and between those of the surface and bulk particles. F-c shows the pattern of the EP ( $-300$  mesh) sample with carbon (C/EP = 0.5) which has been heated up to  $960^\circ\text{C}$  by the chlorination-DTA in a  $\text{Cl}_2$  flow. It is shown that the peak strength of mullite reduces after the chlorination.

Figure 7 shows the X-ray diffraction patterns before and after the chlorination of the samples (C/sample = 0.5) which were prepared by the mullitization reaction of the mixture (3:2) of activated alumina ( $-300$  mesh) and amorphous silica ( $-300$  mesh). Precipitated silicic anhydride (Kanto, GR) was used as  $\text{SiO}_2$ . M-a shows the X-ray pattern of the sample prepared by heating the mixture at  $1550^\circ\text{C}$  for 1 h. The mullite shows a higher crystallinity than in F-a of Fig. 6 and the presence of  $\alpha\text{-Al}_2\text{O}_3$  is shown. M-b shows the pattern for the sample used in M-a after it was heated to  $870^\circ\text{C}$  by the chlorination-DTA in a  $\text{Cl}_2$  flow. M-c shows the pattern for the sample, which was prepared by heating the mixture at  $1400^\circ\text{C}$  for 2 h, and was then heated up to  $910^\circ\text{C}$  by the chlorination-DTA in a  $\text{Cl}_2$  flow. There is no significant

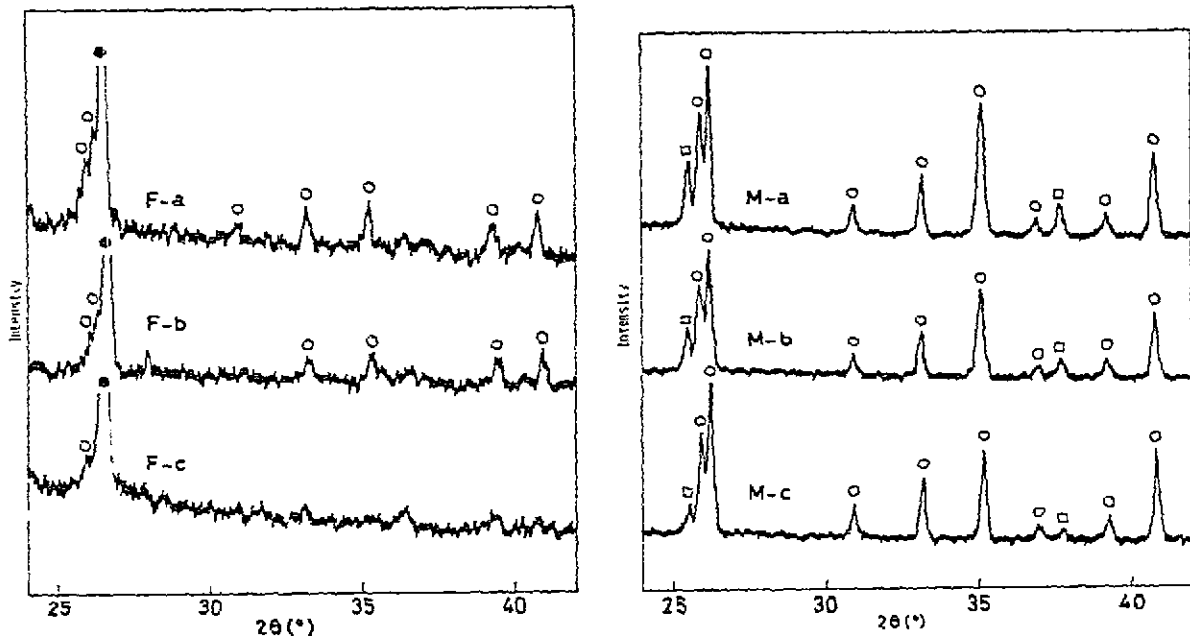


Fig 6 X-Ray diffraction patterns of fly ash before and after the chlorination (Cu-target,  $800 \text{ c s}^{-1}$ ). F-a, original fly ash-EP ( $-300$  mesh) F-b, fly ash-MC ( $-300$  mesh) prepared by grinding MC ( $+100$  mesh). F-c, fly ash-EP ( $-300$  mesh) with carbon (C/EP=0.5) after being heated up to  $960^\circ\text{C}$  by the chlorination-DTA in a  $\text{Cl}_2$  flow. O, mullite, ●, quartz.

Fig 7 X-Ray diffraction patterns of mullite with carbon (C/mullite=0.5) before and after the chlorination (Cu-target,  $2000 \text{ c s}^{-1}$ ). Mullite was prepared by the mullitization of a mixture of  $\text{Al}_2\text{O}_3$  and  $\text{SiO}_2$  (3:2) M-a, mullite prepared at  $1550^\circ\text{C}$  for 1 h. M-b, mullite in M-a after being heated up to  $870^\circ\text{C}$  by the chlorination-DTA in a  $\text{Cl}_2$  flow; M-c, mullite prepared at  $1400^\circ\text{C}$  for 2 h, after being heated to  $910^\circ\text{C}$  by the chlorination-DTA in a  $\text{Cl}_2$  flow. O, mullite □,  $\alpha\text{-Al}_2\text{O}_3$

difference between the patterns of M-a, M-b and M-c, in contrast with the result for fly ash in Fig. 6. On the basis of these results, the reactivity of mullites towards chlorination depends on their crystallinity differences resulting from the preparative temperature.

Figure 8 shows the X-ray patterns before and after the chlorination of mullite prepared by calcining kaolin. M-d shows the pattern of the sample prepared by calcining kaolin at  $1400^\circ\text{C}$  for 2 h in air. The peaks of mullite and cristobalite are recognized. M-e shows the pattern of the sample of M-d with carbon (C/sample = 0.5) after being heated to  $940^\circ\text{C}$  by the chlorination-DTA in  $\text{Cl}_2$ . Reduction in the peak height of mullite is recognized. This is probably due to the chlorination of mullite and to the dilution of the mullite concentration by adding carbon. M-f shows the pattern of the sample prepared by calcining kaolin at  $1200^\circ\text{C}$  for 1 h, and this is in good agreement with that of EP ( $-300$  mesh) in F-a. Compared with M-d, the crystallinity of mullite is low and peaks of quartz appear instead of cristobalite. M-g shows the pattern of the sample of M-f with carbon (C/sample = 0.5) after being heated to  $900^\circ\text{C}$  by the chlorination-DTA. The peaks of mullite become smaller than

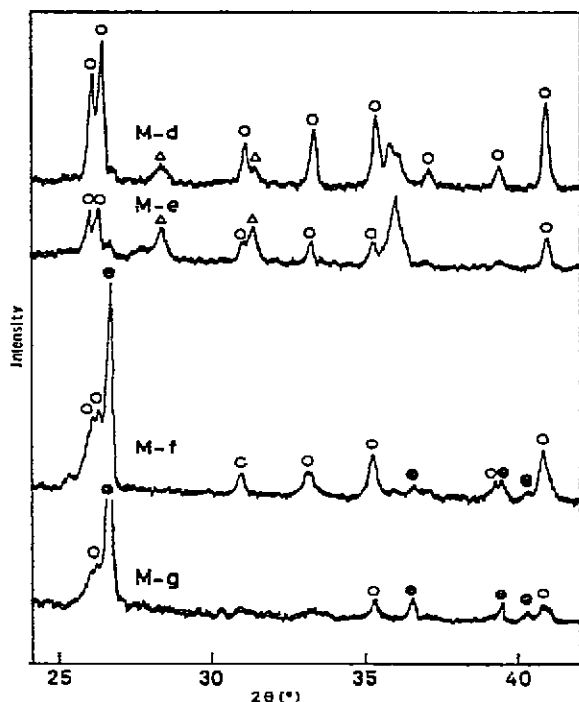
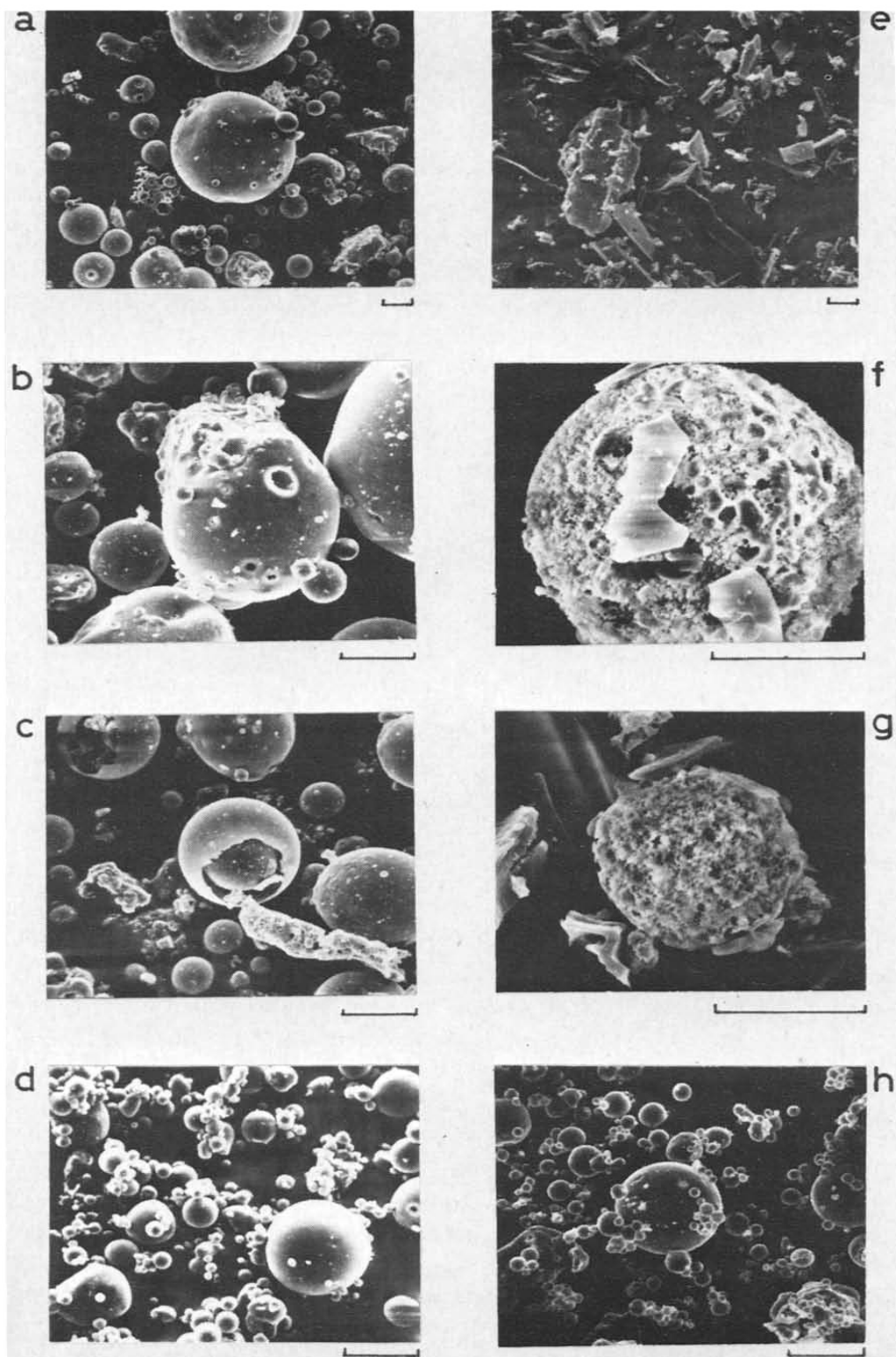


Fig. 8 X-Ray diffraction patterns of mullite prepared by calcining kaolin M-d, mullite prepared at 1400°C for 2 h; M-e, mullite of M-d with carbon (C/mullite=0.5) after being heated to 940°C by the chlorination-DTA in a Cl<sub>2</sub> flow; M-f, mullite prepared at 1200°C for 1 h; M-g, mullite of M-f with carbon (C/mullite=0.5), after being heated to 900°C by the chlorination-DTA in a Cl<sub>2</sub> flow ○, mullite, ●, quartz, △, cristobalite (Cu-target, 2000 c s<sup>-1</sup>)

those in M-f, and the chlorination is much more extensively promoted than M-e. These results also suggest that the reactivity of crystalline mullite in fly ash towards the chlorination depends on its preparative temperature.

Figure 9 shows the scanning electron micrographs of fly ash before and after the chlorination. A scale shown below each micrograph corresponds to 20 μm in length. (a) shows fly ash-MC (-100 +200 mesh) which is widely distributed from 90 to 5 μm in diameter. The particles are spheres with a smooth surface, but it also contains partly non-spherical or porous material. (b) shows fly ash-MC (-200 +300 mesh). A large particle in the center is about 50 μm in diameter, having a hole in the crater-like structure. (c) shows fly ash-MC (-300 mesh). A spherical particle ( $d = 35 \mu\text{m}$ ) located in the center includes another small particle ( $d = 20 \mu\text{m}$ ). (d) shows fly ash-EP (-300 mesh), which is almost all smooth spherical particles and with diameters widely distributed from 30 to 3 μm. (e) shows the active carbon used as a reducing agent. (f) shows the fly ash-MC (-200 +300 mesh) with carbon (C/MC = 0.5) heated up to 940°C by the chlorination-DTA in a Cl<sub>2</sub> flow. The surface of the spherical particle ( $d = 50 \mu\text{m}$ ) undergoes a vigorous erosive action during the chlorination reaction. The materials located on the particle are active carbon. The promoting mechanism of the carbon on chlorination is not understood in detail, but



**Fig 9** SEM photographs of fly ash before and after the chlorination. Each scale corresponds to 20  $\mu\text{m}$  in length. a, fly ash-MC (-100 +200 mesh). b, fly ash-MC (-200 +300 mesh). c, fly ash-MC (-300 mesh). d, fly ash-EP (-300 mesh). e, active carbon; f, fly ash-MC (-200 +300 mesh) with carbon, after being heated to 940°C by the chlorination-DTA in a  $\text{Cl}_2$  flow; g, fly ash-EP (-300 mesh) with carbon, after being heated to 956°C in a  $\text{Cl}_2$  flow; h, fly ash-EP (-300 mesh) without carbon, after being heated to 900°C by the chlorination-DTA in a  $\text{Cl}_2$  flow.

it is interesting that carbon in a contact state as shown in the photograph promotes the reaction. (g) shows the fly ash-EP (-300 mesh) with carbon ( $C/EP = 0.5$ ) heated up to  $956^{\circ}\text{C}$  by the chlorination-DTA in a  $\text{Cl}_2$  flow. The surface of the spherical particle ( $d = 30\ \mu\text{m}$ ) undergoes an erosive action as in (f). (h) shows fly ash-EP (-300 mesh) without carbon ( $C/EP = 0$ ) heated up to  $900^{\circ}\text{C}$  by the chlorination-DTA in a  $\text{Cl}_2$  flow. No change in the surface of the particles means that no chlorination reaction occurs.

Figure 10 shows the electron microprobe X-ray images of the elemental Si and Al in fly ash-MC (+100 mesh). (i) shows the electron image of the particles distributed from 200 to  $100\ \mu\text{m}$  in size. (j) shows the enlarged photograph of the cross section of materials located at the right side of (i). It is shown that the inside of the spherical particle is empty. (k) shows the component distributions of elemental Si and Al, which were obtained by the line-analysis along the A-B line in (j). (l) and (m) show the Si- $\text{K}\alpha$  and Al- $\text{K}\alpha$  images, respectively. On the basis of these results, it is thought that Si and Al distribute homogeneously in a typical spherical fly ash particle.

#### *Chlorination-DTA of bauxite*

Figure 11 shows the SEM photograph of bauxite (-200 mesh). The particles of bauxite differ greatly from fly ash, having a glassy smooth spherical surface.

Figure 12(A) shows the chlorination-DTA curves of bauxite, with gibbsite and hematite as constituents. (a) shows the DTA curve of bauxite with carbon ( $C/\text{bauxite} = 0.5$ ) in a  $\text{Cl}_2$  flow. Two exothermic peaks appear at about  $270$  and  $490^{\circ}\text{C}$ . From the fraction of iron and aluminum converted in the chlorinated samples which were taken out at various temperatures marked on curves (a) and (b), (part (B) in this figure), it is thought that these peaks correspond to the chlorination reactions of iron and aluminum in the bauxite ore, respectively. However, the peak at  $270^{\circ}\text{C}$  is abnormally large, compared with the peak at  $490^{\circ}\text{C}$  corresponding to the chlorination of aluminum. (c) shows the DTA curve of the bauxite with carbon ( $C/\text{bauxite} = 0.5$ ) in a  $\text{N}_2$  flow. Only one endothermic peak corresponding to the dehydration of gibbsite as a constituent of bauxite appears at about  $320^{\circ}\text{C}$ . (b) shows the DTA curve of the dehydrated bauxite (obtained at  $380^{\circ}\text{C}$  on run c) with carbon ( $C/\text{bauxite} = 0.5$ ) in a  $\text{Cl}_2$  flow. The exothermic peak corresponding to the chlorination of iron at about  $290^{\circ}\text{C}$  is smaller than that of (a), and the peak corresponding to the chlorination of aluminum shifts to a slightly higher temperature. The behavior of the fractional conversions in part (B) corresponds to that of curve (a). On the basis of these data, it is thought that the large exothermic peak at about  $270^{\circ}\text{C}$  in curve (a) was generated under the influence of the water resulting from the dehydration of the gibbsite in bauxite. It is presumed that this enormous exotherm is due to the overlapping of some exothermic reaction, the formation of hydrogen chloride by the reaction of water with chlorine in the presence of carbon [2], with the endotherm for the dehydration of gibbsite. (d) shows the DTA curve of bauxite alone in a  $\text{Cl}_2$  flow. It is seen that no chlorination reaction occurs in the system without carbon at a temperature below  $600^{\circ}\text{C}$ . (e) shows the DTA curve of

100

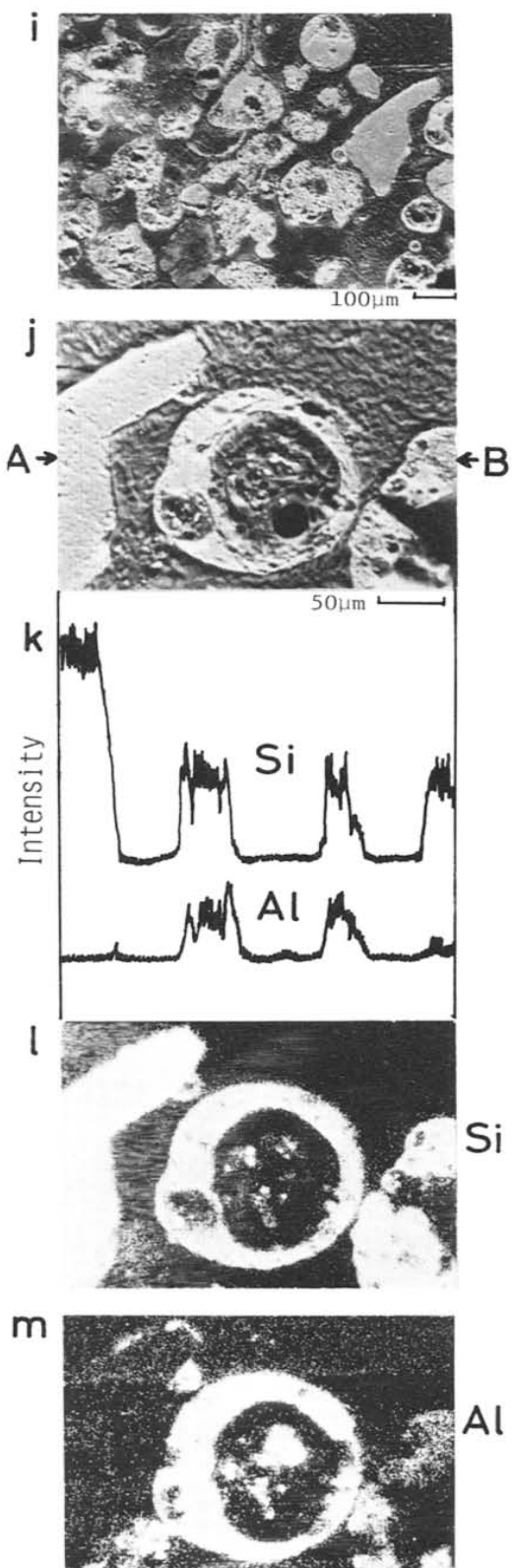


Fig. 10 EPMA images of fly ash-MC (+100 mesh) i, electron image of particles; j, enlarged photograph of the material located at the right side of i, k, component distributions of Si and Al elements along the A-B line in j; l, Si-K $\alpha$  image; m, Al-K $\alpha$  image.

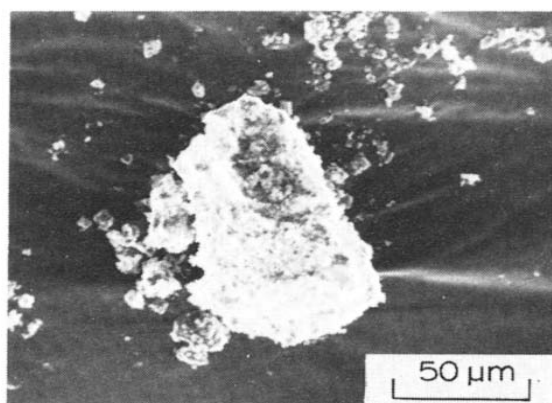


Fig 11. SEM photograph of bauxite ( $-200$  mesh)

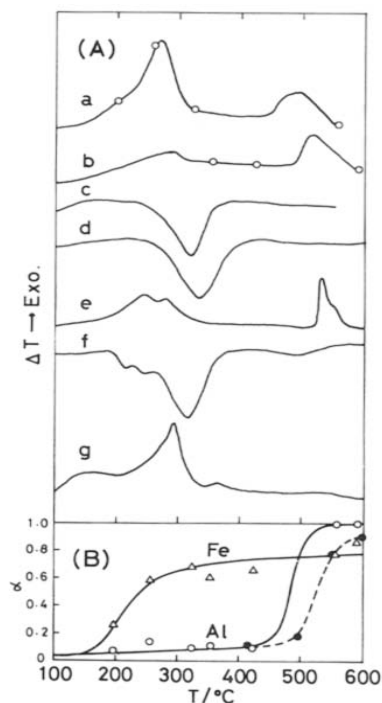


Fig 12 (A) DTA curves of bauxite, gibbsite and hematite in a  $\text{Cl}_2$  or  $\text{N}_2$  flow a, bauxite with carbon ( $\text{C}/\text{bauxite}=0.5$ ) in  $\text{Cl}_2$ , b, dehydrated bauxite (obtained at  $380^\circ\text{C}$  on run c) with carbon ( $\text{C}/\text{bauxite}=0.5$ ) in  $\text{Cl}_2$ , c, bauxite with carbon ( $\text{C}/\text{bauxite}=0.5$ ) in  $\text{N}_2$  flow, d, bauxite alone in  $\text{Cl}_2$ , e, gibbsite with carbon ( $\text{C}/\text{gibbsite}=0.5$ ) in  $\text{Cl}_2$ ; f, gibbsite alone in  $\text{Cl}_2$ ; g, hematite with carbon ( $\text{C}/\text{hematite}=0.5$ ) in  $\text{Cl}_2$  (B). The fraction of Fe and Al converted by chlorination in the samples taken out at the various temperatures in curves (a) and (b), and of gibbsite with carbon ( $\text{C}/\text{gibbsite}=0.5$ )  $\Delta$ , Fe;  $\circ$ , Al,  $\bullet$ , gibbsite

gibbsite with carbon ( $\text{C}/\text{gibbsite}=0.5$ ) in a  $\text{Cl}_2$  flow. The exothermic peak at  $200\text{--}300^\circ\text{C}$  seems to be due to the overlapping of an exothermic reaction by water (resulting from the dehydration of gibbsite) with  $\text{Cl}_2$  and carbon, with an endothermic reaction from the dehydration of gibbsite. The exothermic peak at about  $530^\circ\text{C}$  is due to the chlorination of alumina, although this peak shifts to a temperature of about  $40^\circ\text{C}$  higher than that in curve (a). (f) shows the DTA curve of gibbsite alone in a  $\text{Cl}_2$  flow, and this curve was in fair agreement with the curve of gibbsite with carbon in a  $\text{N}_2$  flow [7]. Tsuchida et al. [7] have reported that in the case of the gibbsite with carbon ( $\text{C}/\text{gibbsite}=0.5$ ) in a  $\text{N}_2$  flow a small endothermic peak at  $220\text{--}260^\circ\text{C}$  corresponds to a partial decomposition of gibbsite to boehmite and a large endothermic peak at about  $315^\circ\text{C}$  corresponds to the decomposition of gibbsite to  $\chi\text{-Al}_2\text{O}_3$ . The sample heated up to  $420^\circ\text{C}$  consists of a large amount of  $\chi\text{-Al}_2\text{O}_3$  and a small amount of boehmite which decomposed endothermically to  $\gamma\text{-Al}_2\text{O}_3$  at  $520^\circ\text{C}$ . Therefore, it is considered that the exothermic peak at about  $520\text{--}570^\circ\text{C}$  in curve (e) corresponds to the chlorination of  $\chi\text{-Al}_2\text{O}_3$  (mainly) and  $\gamma\text{-Al}_2\text{O}_3$ . A

difference of peak temperature corresponding to the chlorination of alumina between curves (a) and (e) is probably due to the reactivity difference resulting from the structure or crystallinity of alumina. (g) shows the DTA curve of the hematite with carbon ( $C/\text{hematite}=0.5$ ) in a  $\text{Cl}_2$  flow. An exothermic peak at  $290^\circ\text{C}$  corresponds to the chlorination of hematite.

Figure 12(B) shows the fraction of iron and aluminum converted in the chlorination in the samples taken out at various temperatures in curves (a) and (b). The behavior of iron and aluminum to chlorination correspond well with the exothermic peaks at about  $290^\circ\text{C}$  and  $490\text{--}510^\circ\text{C}$ , respectively. The Fe-curve shows that the reaction attains rapidly to about 65% conversion at  $300^\circ\text{C}$ , but the reaction rate slows to around 80% at  $600^\circ\text{C}$ . On the other hand, the Al-curve shows that the reaction attains to 100% conversion at  $550^\circ\text{C}$ . Furthermore, in this figure the conversion of Al is compared with that of gibbsite [7]. It is seen that this result corresponds well to curve (e), and the reactivity of gibbsite is lower than that present in bauxite.

#### *X-Ray analysis of bauxite*

Figure 13 shows the X-ray diffraction patterns of bauxite before and after heating in air, and after the chlorination in a  $\text{Cl}_2$  flow. B-a shows the X-ray pattern of

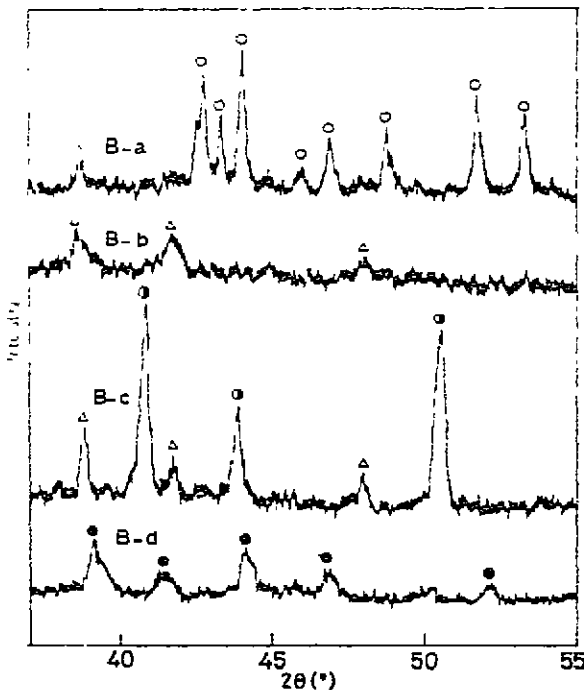


Fig 13 X-Ray diffraction patterns of bauxite before and after being heated in air (Co-target,  $500\text{ c s}^{-1}$ ), and after the chlorination-DTA in a  $\text{Cl}_2$  flow (Cu-target,  $800\text{ c s}^{-1}$ ) B-a, original bauxite, B-b, bauxite heated at  $380^\circ\text{C}$  for 1 h in air, B-c, bauxite heated at  $1100^\circ\text{C}$  for 1 h in air; B-d, mixture of bauxite (in B-a) with carbon ( $C/\text{bauxite}=0.5$ ) heated up to  $575^\circ\text{C}$  by the chlorination-DTA in a  $\text{Cl}_2$  flow and condensates deposited on the cool end of the cell. ○, gibbsite; Δ,  $\alpha\text{-Fe}_2\text{O}_3$ ; ●,  $\alpha\text{-Al}_2\text{O}_3$ ; ■,  $\text{AlCl}_3 \cdot 6\text{H}_2\text{O}$ .

original bauxite. The peaks corresponding to gibbsite and  $\alpha\text{-Fe}_2\text{O}_3$  (low crystallinity) are recognized. B-b shows the pattern of the bauxite heated at  $380^\circ\text{C}$  for 1 h in air. The peaks of gibbsite disappear and those of  $\alpha\text{-Fe}_2\text{O}_3$  enlarge. B-c shows the pattern of the bauxite heated at  $1100^\circ\text{C}$  for 1 h in air. The peaks of  $\alpha\text{-Al}_2\text{O}_3$  newly appear and those of  $\alpha\text{-Fe}_2\text{O}_3$  become progressively greater. B-d shows the pattern (measured by  $\text{CuK}\alpha$ ) of the mixture of bauxite (in B-a) with carbon ( $\text{C}/\text{bauxite} = 0.5$ ), heated up to  $575^\circ\text{C}$  by the chlorination-DTA in a  $\text{Cl}_2$  flow and condensates deposited on the cool end of the cell. Only the peaks of  $\text{AlCl}_3 \cdot 6\text{H}_2\text{O}$  are recognized. Since there was no diffraction peak in the chlorinated bauxite at  $575^\circ\text{C}$ , it is considered that the  $\text{AlCl}_3$  formed sublimed and condensed on the cool end of the cell.

#### ACKNOWLEDGEMENTS

The authors wish to thank Dr. T. Okutani, Government Industrial Development Laboratory, Hokkaido, for EPMA observations, and Mr. K. Takahashi, Hokkaido Electric Power Co., for supplying the samples of fly ash.

#### REFERENCES

- 1 H S Simons and J W Jeffery, *J Appl Chem*, 10 (1960) 328
- 2 D C Cavin, W A Klemm and G Burnet, *Proc. Iowa Acad Sci*, 81 (1974) 130
- 3 A Landsberg, *Metall Trans*, 6B (1975) 207.
- 4 M J Murtha and G Burnet, *Proc Iowa Acad Sci*, 83 (1976) 125
- 5 A K Mehrotra, P R Bishnoi and W Y Srceek, *Can J Chem Eng.* 57 (1979) 225
- 6 T. Ishii, R Furuichi and Y Kobayashi, *Thermochim Acta*, 9 (1974) 39
- 7 T Tsuchida, T Ishii, R Furuichi and H Haga, *Thermochim Acta*, 34 (1979) 19
- 8 T Ishii, R Furuichi and K Kudo, *Netsusokuter*, 4 (1977) 100
- 9 JIS, M8815-1976, *Methods for Analysis of Coal Ash and Coke Ash*, 1976
- 10 JIS, A6201-1977, *Fly Ash*, 1977.
- 11 B B Ghate, D P H Hasselman and R M Spriggs, *Ceram Bull*, 52 (1973) 670
- 12 JIS, M8361-1968, *Methods for Chemical Analysis of Bauxite Ores*, Japan, 1968
- 13 Y Okahara and I Iwasaki, *Trans AIME*, 247 (1970) 73